NASA Technical Memorandum 85834

COMPRESSION FAILURE MECHANISMS IN UNIDIRECTIONAL COMPOSITES

H. Thomas Hahn

AND

Jerry G. Williams

August 1984

National Aeronautics and
Space Administration

Langley Research Center
Hampton, Virginia 23665

COMPRESSION FAILURE MECHANISMS IN UNIDIRECTIOINAL COMPOSITES

H. Thomas Hahn
Department of Mechanical Engineering
and Materials Research Laboratory
Washington University
St. Louis, MO 63130

Jerry G. Williams
National Aeronautics And Space Administration
Langley Research Center
Hampton, VA 23665

SUMMARY

The present paper examines compression failure mechanisms in unidirectional composites. Possible failure modes of constituent materials are summarized and analytical models for fiber microbuckling are reviewed from a unified viewpoint. Due to deficiencies in available models, a failure model based on nonlinear material properties and initial fiber curvature is proposed.

The effect of constituent properties on composite compression behavior was experimentally investigated using two different graphite fibers and four different epoxy resins. The predominant macroscopic-scale failure mode was found to be shear crippling. In a soft resin, shear crippling was in the form of buckling of fibers on a microscopic scale. However, for stiff resins failure was characterized by the formation of a kink band. For unidirectional laminates, compressive strength, and compressive modulus to a lesser extent, were found to increase with increasing magnitude of resin modulus. The change in compressive strength with resin modulus was predicted using the proposed nonlinear model.

INTRODUCTION

The inherent weakness of current graphite-epoxy composites to impact and delamination has prompted the development of improved material systems through the use of tougher resins and higher strain fibers [1,2]. Present technology, however, is limited in that improved toughness has in general been accompanied by a sacrifice in other properties such as strength and stiffness at elevated-temperature. The longitudinal compressive strength of unidirectional composites depends on many factors including the stiffness and strength of the matrix and fiber. Better understanding of compressive failure mechanisms is needed to more accurately predict strength changes resulting from the use of different resins and fibers.

Over the past two decades, much effort has been concentrated on understanding the failure mechanisms and predicting the strength of compression loaded laminates. Since fracture of composites is usually instantaneous and catastrophic, identification of critical failure modes is not easily accomplished. The problem is complicated because changes in material properties or the presence of defects can lead to completely different failure modes. Thus, an analytical model accurate for one material system may not predict failure for another material system. Development of a unified model which can be applied to various material systems and failure modes is not within grasp at present. The current approach is to identify critical failure modes for each material system and to develop a unique model for each failure mode.

The present paper reviews failure modes in and analytical models for unidirectional composites subjected to longitudinal compression loading. The results of an experimental investigation on the effect of constituent material properties on compression behavior are discussed and compared with other available data. A possible sequence of failure initiation and propagation is proposed based on observations made during testing and from the examination of failed specimens.

BACKGROUND ON FAILURE MODES

Failure Modes of Fibers

The compressive failure characteristics of a fiber can be studied by embedding it in a resin casting [3]. The transparency available in an epoxy resin and the high axial stiffness of a large cross-section of resin relative to the fiber makes it possible to monitor the controlled failure of the fiber during loading. Compression failure modes characteristic of a fiber bundle have also been successfully observed using transparent resins to encapsulate the fibers [4].

Fibers fail differently depending on their internal structure, Fig. 1. High-modulus graphite fibers fracture in shear along a maximum shear plane [3]. The initiation of fracture is usually in the form of a hairline crack around the fiber circumference. The crack grows inward from the surface layer fairly normal to the fiber axis. However, final failure is along a maximum shear plane. Higher modulus is the result of better alignment of internal structure, and is associated with lower compressive failure strain. However, PAN Type II and Type A graphite fibers have been observed not to fracture due to compression loading at strains up to 3 percent [3]. Kevlar fibers, on the other hand, fail in a kink mode because of Kevlar's characteristic weak bond in the radial direction which permits individual fibers to split into fibrils [5].

Both shear failure and fiber kinking are characteristic failure modes for fibers with well-aligned fibrillar structure. The basic mechanisms for the two failure modes seem to be the same; i.e., they are both the result of aligned fibrillar structure and a weak radial bond. However, the low ductility for graphite fibers leads to fracture while the development of fibrils for Kevlar fibers results in kinking.

Brittle fibers with amorphous structure such as glass do not usually fail in the aforementioned failure modes. These fibers can fail in bending, starting from the tension side. Medium to high-strength fibers may also fail in bending.

The failure modes strongly depend upon the lateral support provided the fiber during loading. In the absence of a strong lateral support, all fibers would fail by buckling. As the support stiffness increases, buckling is suppressed and the fiber begins to fail in shear. However, no shear failure has yet been observed for glass fibers or for high-strength graphite fibers such as T300 and T700.

Failure Modes of Resins

Compression tests on bulk resins reveal two types of failure. For ductile resins plastic flow is frequently observed in a broad band oriented ~45 degrees to the loading axis. For brittle resins, however, shear banding, i.e., narrow zones of shear yielding, can precede ultimate failure.

Failure Modes of Composites

Because of the weakness of the matrix and the fiber/matrix interface compared with the strength of the fibers, unidirectional composites can fracture along the fibers even when loaded by compression, Fig. 1. Transverse tensile stresses develop in the matrix due to Poisson's ratio differences between the matrix and fiber, and stress concentrations caused by voids

can initiate fracture in the fiber/matrix interface [6].

If a fiber buckles, the matrix/fiber interface may fracture in shear and lead to ultimate failure. However, if the matrix is ductile and the interface is strong, the fiber can bend without matrix failure and eventually fracture in bending. The eccentricity introduced by such fiber fracture may lead to longitudinal splitting with continued compression loading.

A more likely failure mode of composites associated with fiber buckling and kinking is shear crippling. Macroscopically, shear crippling looks like a shear failure on a plane at an angle to the direction of loading. Microscopic inspection, however, indicates shear crippling is frequently the result of kink band formation, Fig. 2.

Some of the reported values for the kink band boundary angle and the segment length are listed in Table 1 [7-9]. The kink orientation angle α is not well defined because it will depend on the load history. The angle α can be shown to be twice the angle β if no volume change is assumed within the kink band [9].

In graphite fiber composites, fiber breaks are usually observed at the kink band boundaries [8,10] while fiber kinking and extreme fiber bending without fracture are typical for Kevlar and glass composites, respectively [7,9].

The kink bands are most clearly observed when failure is gradual and also when longitudinal splitting is prevented by application of hydrostatic pressure [8]. Gradual failure is also observed when there is a gradient in the stress field, e.g., near a hole [1] or in bending, and when fiber tows are surrounded by matrix as in carbon/carbon composites.

The third failure mode of composites is associated with pure compression failure of fibers. In this case, the fracture surface is likely to be at an angle, about 45 degrees, to the loading. Post-failure examinations of fracture surfaces of graphite/epoxy composites alone is usually inadequate to distinguish between fiber kinking and fiber compression failure because the broken fiber segments resulting from kinking failure are randomly displaced during the catastropic failure event [11].

The available data in the literature strongly suggest that the most likely failure mode in graphite/epoxy composites for strength-critical applications is shear crippling involving fiber kinking. Compression failure of a composite starts with kinking of a few fibers. The kinked fibers disrupt the stability of the neighboring fibers so that the neighboring fibers also fail in the kinking mode. This damage propagation process continues until the composite completely fails. In some cases, fiber kinking may be initiated at several different locations and proceed to converge. The transverse tensile stress in the region where the two advancing kink bands meet may be sufficiently high

to cause longitudinal splitting.

The failure modes discussed thus far depend on various material properties and geometrical parameters. Some properties and parameter values may promote one failure mode while other values may favor another. The effect of material properties and geometrical parameters is qualitatively discussed in the following section.

BACKGROUND ON ANALYTICAL MODELS

General Formulation

Consider a fiber embedded in a continuum. A free-body diagram for an infinitesimal segment of the fiber is shown in Fig. 3. The parameters in the figure are defined as follows:

P = axial compressive force

Q = transverse shear

M = bending moment

p = applied distributed axial force

q = applied distributed transverse force

m = applied distributed bending moment

Assuming small deflection and the initial fiber axis to be along the x axis, we can write the equilibrium equations as [12]

$$q + \frac{dQ}{dx} + P\frac{d\omega}{dx} = 0 \qquad (1)$$

$$p - \frac{dP}{dx} + Q\frac{d\omega}{dx} = 0 \qquad (2)$$

$$\frac{dM}{dx} - Q + m = 0 \qquad (3)$$

where ω is the slope of the deflected fiber axis.

The exact determination of the forces and moments p, q, m, and M is not possible without the knowledge of the displacement fields in the fiber and the surrounding continuum. That is, one must solve the foregoing equations in conjunction with the equilibrium equations for the continuum using the appropriate constitutive relations. Thus, the final solution for the failure load will depend on properties of the constituent materials.

The problem can be simplified if certain assumptions are made for the forces and moments p, q, m and M. Various simplifying assumptions proposed in the literature are reviewed in the following section.

Single Fiber Embedded in Infinite Matrix

The model of a fiber surrounded by infinite matrix has been solved within the framework of elasticity [12-14]. This model approximates the behavior of a composite with a low fiber volume content. The salient features of this model can be studied by way of the following simplified analysis.

The combination of Eqs. (1) and (2) with m = 0 and P = constant leads to

$$\frac{d^2M}{dx^2} + q + P\frac{d^2v}{dx^2} = 0 \tag{4}$$

where v is the transverse deflection of the fiber and $\omega = \frac{dv}{dx}$. Noting that

$$M = E_f I_f \frac{d^2v}{dx^2}, \tag{5}$$

and assuming that

$$v = f \cos \frac{\pi}{\ell} \times \tag{6}$$

$$q = +Kv \ , \ K = \text{constant} \tag{7}$$

gives the buckling load as [12]

$$P_{fc} = 2(KE_f I_f)^{\frac{1}{2}} \tag{8}$$

Here E_f and I_f are the fiber modulus and moment of inertia, respectively.

The corresponding buckle half wavelength is

$$\ell = \pi\left(\frac{E_f I_f}{K}\right)^{\frac{1}{4}} \tag{9}$$

According to the more rigorous solutions [12,14], K is not a constant but depends on ℓ as well as on material properties. However, K is approximately proportional to the matrix modulus E_m [15]. Thus,

$$P_{fc} \propto (E_m E_f I_f)^{\frac{1}{2}} \tag{10}$$

$$\ell \propto \left(\frac{E_f I_f}{E_m}\right)^{\frac{1}{4}} \tag{11}$$

If the interaction between fibers can be neglected, e.g., in composites with low fiber volume content, the resulting buckling strain ε_c of composite is given by

$$\varepsilon_c = \frac{P_{fc}}{E_f A_f} \propto \left(\frac{E_m}{E_f}\right)^{\frac{1}{2}} \tag{12}$$

where A_f is the cross-sectional area of the fiber.

Fiber Buckling in Composites

Since it is difficult to include the exact interaction effect between fibers, a variety of approximations have been attempted for the forces and moments p, q, m, and M based on simplified displacement fields. Furthermore, fibers have frequently been idealized as plates so that a two-dimensional analysis could be applied.

If two neighboring fibers are assumed to buckle out of phase with each other, the foundation constant K may be assumed to be [16,17]

$$K = 4 \frac{E_m}{h_m} \tag{13}$$

where h_m is the thickness of the matrix layer. The corresponding buckling load in the fiber is obtained by substituting Eq. (13) into Eq. (8). The composite failure stress then follows from the rule of mixtures, i.e.,

$$\sigma_c = v_f \sigma_{fc} = v_f \frac{P_{fc}}{A_f} \tag{14}$$

where v_f is the fiber volume content.

Another simple displacement field is associated with fibers

buckling in phase. Since all fibers deform the same way, one can assume [16,17] (cf. Appendix for m)

$$p = q = 0 \tag{15}$$

$$m = -\frac{h_f}{v_f}\frac{G_m}{1-v_f}\frac{dv}{dx} \tag{16}$$

where h_f is the thickness of the fiber layer. The resulting equation of equilibrium is then

$$\frac{d^2M}{dx^2} + \frac{dm}{dx} + P\frac{d^2v}{dx^2} = 0 \tag{17}$$

Substitution of Eqs. (5), (6), and (16) into Eq. (17) yields

$$P_{fc} = \frac{h_f}{v_f}\frac{G_m}{1-v_f} + E_f I_f \left(\frac{\pi}{\ell}\right)^2 \tag{18}$$

The corresponding composite buckling stress is thus (cf. Eq. (14))

$$\sigma_c = \frac{G_m}{1-v_f} + v_f \frac{E_f I_f}{h_f}\left(\frac{\pi}{\ell}\right)^2 \tag{19}$$

If $h_f \ll 1$, Eq. (19) reduces to

$$\sigma_c = \frac{G_m}{1-v_f} \tag{20}$$

Equation (19) is generally known to yield a much higher strength than is realized experimentally. Many improvements and modifications have been suggested over the years [7,18-23]. Most improvements try to incorporate initial curvature of fibers and material nonlinearity. These improvements will be discussed in the following development of a nonlinear model.

Nonlinear Model

A nonlinear model including initial fiber curvature and matrix material nonlinearity is developed using the distributed moment m calculated from the average shear stress field. Assuming an initial deflection of the form

$$v_o = f_o \cos\frac{\pi}{\ell}x \tag{21}$$

one can calculate M, m and q as (cf. Appendix)

$$M = E_f I_f \frac{d^2}{dx^2}(v - v_o) \tag{22}$$

$$m = -\pi \frac{d_f^2}{4} \tau_{LT} = -\pi \frac{d_f^2}{4} G_{LT} \frac{d}{dx}(v - v_o) \tag{23}$$

$$q = +K(v - v_o) \tag{24}$$

Here, G_{LT} is the composite shear modulus, and τ_{LT} and γ_{LT} are the average shear stress and strain, respectively. The fiber diameter is denoted by d_f. In the case of nonlinear stress-strain relations, G_{LT} is taken as the secant modulus at a given γ_{LT}.

The derivation starts with the following equation of equilibrium,

$$\frac{d^2M}{dx^2} + \frac{dm}{dx} + q + P\frac{d^2v}{dx^2} = 0 \tag{25}$$

Substitution of Eqs. (22) - (24) together with Eqs. (6) and (21) into (25) yields

$$\sigma_c = v_f\left[G_{LT} + \frac{E_f I_f}{A_f}\left(\frac{\pi}{\ell}\right)^2 + \frac{K}{A_f}\left(\frac{\ell}{\pi}\right)^2\right]\left(1 - \frac{f_o}{f}\right) \tag{26}$$

Using the condition that σ_c be a minimum at fixed f_o/f and expressing f in terms of G_{LT}, one obtains

$$\sigma_c = v_f\left[G_{LT} + \sqrt{\frac{KE_f}{\pi}}\right]\frac{\gamma_{LT}}{\gamma_{LT} + \pi f_o/\ell} \tag{27}$$

If K is neglected, as is frequently done, σ_c is given by

$$\sigma_c = v_f G_{LT}\frac{\gamma_{LT}}{\gamma_{LT} + \pi f_o/\ell} \tag{28}$$

Furthermore, if no initial defect is assumed, i.e., $f_o/\ell = 0$, one has

$$\sigma_c = v_f G_{LT} \tag{29}$$

Even when G_{LT} is approximated by $G_m/(1-v_f)$, Eq. (29) is different from Eq. (20) by the factor v_f. The difference derives from the selection of the free body. If the free body includes both a fiber and matrix, Eq. (29) without the fiber volume content v_f results [18]. If only a fiber is taken as the free body, Eq. (29) follows. Since Eq. (20) is known to overpredict the strength and because applying the equilibrium forces and moments to the fiber is a reasonable model, Eq. (29) is preferred to Eq. (20).

The importance of initial fiber curvature has been pointed out and incorporated in the model by many investigators [19-23]. The results are all similar to Eq. (28) without the factor v_f.

Since G_{LT} is in general a function of γ_{LT}, Eq. (29) should be solved for a maximum value of σ_c over the allowable range of γ_{LT}. For example, if the shear stress-strain relation can be approximated as that of an elastic-perfectly plastic material with yield stress τ_y, Eq. (28) reduces to

$$\sigma_c = v_f \frac{\tau_y}{\gamma_y + \pi f_o/\ell} \tag{30}$$

If fibers are weak, then fibers may fail before the matrix and interfaces fail in shear. The factor $(1 - \frac{f_o}{f})$ in Eq. (26) can be related to the flexural strength σ_f of the fibers. The result is then

$$\sigma_c = v_f \frac{G_{LT}}{1 + \frac{\pi}{2}\frac{E_f}{\sigma_f}\frac{d_f}{\ell}(\frac{\pi f_o}{\ell})} \tag{31}$$

Equation (31) is likely to be applicable to Kevlar/epoxy composites because the flexural strength of Kevlar fibers is very low.

The effect of a partial bond can be included by introducing a bond efficiency factor for m in Eq. (16) [7]. The interfacial strength and voids reduce the composite shear strength, i.e., the

maximum value of γ_{LT} in Eq. (28). Thus, Eqs. (28) and (31) incorporate most of the important parameters.

The models discussed so far are essentially one-dimensional. A two-dimensional analysis is required to predict the kink band geometry [21]. The analytical results of [21] indicate that the kink band boundary angle becomes zero as σ_c approaches G_{LT}.

EXPERIMENTAL PROCEDURE

Two different fibers were combined with four different resins to make seven unidirectional $[0]_{24}$ graphite/epoxy composites. Specific constituent materials as well as respective fiber weight contents and nominal thicknesses of cured panels are listed in Table 2. Nominal properties of the constituent materials available in the literature are listed in Table 3. The panels were fabricated at the NASA Langley Research Center according to manufacturers' suggested cure cycles.

Compression testing was done on an Instron machine at a crosshead speed of 1 mm/min. Specimens were prepared for testing in an IITRI (Illinois Institute of Technology Research Institute) compression fixture according to procedures described in ASTM test standard D-3410-82.

Specimens were monitored during test for indications of failure through a stereo optical microscope at magnifications up to 100X. Some specimens had one edge polished to monitor failure initiation.

Two specimens from each material system were tested with a strain gage mounted on one surface. When an anomaly was detected in the stress-strain curve, the specimen was unloaded and examined for damage. Failed specimens were examined on optical microscopes at magnifications up to 300X.

RESULTS AND DISCUSSION

Compressive Properties

Strength data for the graphite/epoxy composites are shown in Figs. 4 and 5, where N is the total number of specimens and i is the ordinal number of strength. Of all the composites, scatter is highest for the T300/5208 material, however, this variation is consistent with that reported for this material in Ref. [24]. The strength of the other composite materials show much less variation.

The graphite/epoxy composites are compared with one another

in Fig. 6 for average strength, failure strain, and modulus. In the figure, E is the initial tangent modulus and E_t is the tangent modulus at failure. For the properties other than average strength each point represents one specimen since only two specimens were strain-gaged for each composite material system. The properties measured for T300/5208 are comparable with those reported in [24,25]. The highest strengths on initial moduli are recorded for the T300/4901/MDA and T300/4901/mPDA specimens. The tangent modulus at failure varies much less from material to material than does the initial tangent modulus.

The effect of resin tension modulus on the composite strength and axial modulus is shown in Fig. 7. According to the rule of mixtures the composite modulus E_c is given by

$$E_c = v_f E_f + v_m E_m \tag{32}$$

The rule-of-mixtures prediction based on the maximum variation of constituent properties from Table 1 is shown in Fig. 7. For a laminate with a 60 percent fiber volume fraction, a change of resin modulus from 3 to 5.5 GPa will result in an increase in composite modulus of 1 GPa. This increase is insignificant in comparison to the original composite modulus magnitude which is on the order of 100 GPa. Thus, the observed modulus increase in Fig. 7 is much higher than predicted by Eq. (32).

To ascertain the dependence of compressive modulus of a composite on the resin tensile modulus, the experimental results of Ref. [26] for tensile and compressive moduli for a large number of material systems are plotted in Fig. 8. Linear regression analyses were performed on the data and the results are also shown in the figure while the appropriate parameters are listed in Table 4.

One of the two features that stand out in Fig. 8 is that the compressive modulus of a composite is more dependent on the resin modulus than is the tensile modulus. The other feature is that the composite tensile modulus is greater than the composite compressive modulus for resin modulus values less than approximately 5 GPa.

Precise theories which explain the lower composite modulus in compression than in tension are not available. One possible explanation is that the fibers themselves are less stiff in compression than in tension. The strain hardening observed for graphite/epoxy composites under tension is attributed to improved alignment of internal structure of the graphite fibers during loading. Conversely, initially imperfect alignment of the fiber structure may grow in amplitude during compression loading. However, the change of fiber stiffness alone does not explain the dependence of the composite compressive modulus on the resin modulus.

Another reason may be that the fibers themselves are not perfectly aligned within the lamina. Under compression, the initial misalignment and initial curvature of the fibers may impose disproportionately high stress on the matrix, locally pushing the matrix into the nonlinear range at an early stage of loading. This same argument can also be used to explain strain hardening in tension. A fiber bundle embedded in resin is like a beam-column supported on an elastic foundation which can buckle in uniform wavelength when the resin is soft [4].

Stress-strain curves for the seven materials studied in this investigation are shown in Fig. 9. All of the materials exhibit strain softening with T700/BP907 showing the most nonlinearity. The T300/BP907 specimen that shows an abrupt drop in strain while under constant stress was unloaded before final failure and was examined to reveal a shear crippling failure on one of the edges. The shear crippling occurred outside the region where the strain gage was attached. The sudden decrease in the measured strain is believed to be the result of local microbuckling triggering the initiation of shear crippling.

Stress-strain curves of all the other materials are smooth and provide no indication of subcritical local failure. It seems that the shear crippling in T300/BP907 was subcritical because it occurred at a low stress level. In the other composites, local shear crippling did not occur until the laminate was highly stressed and led to the immediate catastrophic failure of the specimen.

The average compressive strengths for the materials tested from Fig. 6 are replotted in Fig. 7 as a function of the resin tensile modulus. The general trend is that compressive strength increases with increasing resin modulus for the range of values studied. The increase in compressive strength with resin tensile modulus is also characteristic of the data taken from Ref. [26], Fig. 10. As expected, tensile strength is not appreciably affected by the resin modulus. A linear regression analysis conducted on the data from Ref. [26] is presented in Table 4. The regression parameters confirm a strong correlation between compressive strength and resin modulus but a weak correlation between tensile strength and resin modulus.

The current theory represented by Eq. (28) was used to predict compressive strength as a function of the resin modulus. To use Eq. (28) to predict compressive strength requires the parameter f_o/ℓ to be known. Since the full stress-strain relations are not known for most of the materials in Fig. 10, G_{LT} is taken to be the initial modulus for the composite and f_o/ℓ is calculated using representative properties in Eq. (28). The

initial shear modulus G_{LT} is calculated by [27]

$$\frac{1}{G_{LT}} = \frac{v_f}{G_f} + \frac{\eta(1 - v_f)}{G_m} \tag{33}$$

$$\eta = \frac{1}{2}\left(1 + \frac{G_m}{G_f}\right) \tag{34}$$

where G_f is the longitudinal shear modulus of the fiber. For T300/5208 the necessary shear moduli are

$$G_f = 12.4 \text{ GPa}, \qquad G_m = 1.48 \text{ GPa}$$

Using $\sigma_c = 1.56$ GPa for $v_f = 0.6$, one calculates $\frac{f_o/\ell}{\gamma_{LT}} = 0.295$

Thus, if $\gamma_{LT} = 1$ percent, f_o/ℓ is only 0.295 percent which is very difficult to measure.

For the other resins, $(f_o/\ell)/\gamma_{LT}$ was also assumed to be 0.295 and G_m was calculated from E_m under the assumption of an isotropic material with a Poisson's ratio of 0.35. The resulting compression strengths predicted by Eq. (28) are presented in Fig. 10. Under these assumptions, Eq. (28) is seen to overestimate the composite compressive strength when the matrix resin tensile modulus is less than 3 GPa, but in general is in reasonable agreement with observed experimental data.

Lower compressive strength resulting from lower resin modulus also leads to lower flexual strength, as shown in Fig. 11 by the data taken from Ref. [26]. The reason is that, when a composite is weaker in compression, failure will be initiated on the compression side in a flexure test and hence the flexural strength reflects the compressive strength. Flexural strength does not show as good a correlation with resin modulus as does compressive strength. However, the slope of the linear regression line for flexural strength (Fig. 11) is almost the same as for compressive strength, Table 4.

Compressive failure strains obtained by dividing the failure stresses by the corresponding moduli are presented in Fig. 12. The curve in the figure presents a prediction for buckling strain by the Euler equation for a column with clamped ends, i.e., [28]

$$\varepsilon_c = \frac{\pi^2}{3}\frac{1}{(L/h)^2} \tag{35}$$

where L and h are the length and thickness, respectively, of the column. The T300/BP907 and T700/BP907 specimens had tapered tabs, and hence the entire range of possible gage length is shown. All the experimental compressive failure strains are far below the predicted Euler buckling strain.

Failure Modes

With the exception of one T300/5208 specimen and two T300/BP907 specimens, all compression specimens failed suddenly without warning. Monitoring of the polished edge during the test at magnifications up to 50X did not reveal any sign of damage before ultimate failure. Several specimens were loaded in a stepwise manner and examined under a constant load at each step. Other specimens were loaded and then unloaded for examination. No damage was detected following any of these procedures.

The T300/5208 specimen for which failure was arrested is shown in Fig. 13. The shear crippling did not occur across the entire width since the opposite edge remained intact. Details of the right end of the upper failure are shown in Fig. 13(b). Most of the broken fiber segments in the kink band are gone, but the few remaining ones are seen to be of short length and tilted. The curvature in the fibers below the secondary kink band is required for kinematic compatibility.

The failure mode observed for a T300/BP907 specimen is shown in Fig. 14. The buckle mode shape is well defined and multiple fractures of the fiber are observed within the buckle region. This is in contrast to the kink band failure mode in which two fractures occur per fiber and the short broken fibers align in a regular parallel pattern rotated relative to the direction of the applied compression load, Fig. 13. In Fig. 14, the band of microbuckling appears to have started at the left edge and grown into the interior of the specimen. The pattern of failure in Fig. 14(c) suggests that the microbuckling of fibers may start with the buckling of a single fiber and progressively involve additional fibers as the damage propagates. Microbuckling causes a tensile stress to develop in the matrix between the buckled and the adjacent straight fiber which reduces the applied load at which the adjacent straight fiber buckles. Microbuckling is more likely to initiate at a free edge than in the interior because the lateral support to the fiber is lower in this region. Microbuckling, however, can also develop in the interior of a laminate in regions of voids or where the fiber-to-matrix bond is defective.

Fracture surfaces of failed specimens did not show much variation for the material systems studied. Shear crippling was observed both through the width, Fig. 15(a) and through the

thickness, Fig. 15(b). Partial shear crippling sometimes caused longitudinal splitting, Fig. 13. Shear crippling could occur on several planes just like slip lines in elasto-plastic materials, Fig. 15(a).

The failure sequence for unidirectional composites is proposed as follows. As the compression load is increased, the weakest fibers or the fibers that have the least lateral support because of a free boundary, poor fiber to matrix bond, or voids fail first. The failure initiation may also be due to the stress concentrations introduced by test hardware. For the graphite/epoxy composites studied, the failure takes the form of kinking if the matrix is stiff, or of microbuckling if the matrix is soft. Fiber kinking is distinguished from fiber microbuckling in that the former involves the formation of a regular kink band pattern oriented at less than 90 degrees to the direction of the applied load while microbuckling failure involves large post buckling deformations of the fiber in which multiple fractures may occur due to the high bending strains. In both cases, however, failure observed on the macroscopic scale for unidirectional composites, i.e., looking at a free edge, normally is characterized by shear crippling involving narrow failure zones oriented at less than 90 degrees relative to the applied load. Multiple shear crippling zones may develop in a specimen and the transverse tensile stress which develops in the matrix, particularly as failed fibers become wedged between fibers, may cause matrix fractures to propagate parallel to the fibers.

CONCLUSIONS

The compression behavior of unidirectional graphite/epoxy composites was studied using two different fibers and four different resin systems. The fibers were T300 and T700 whereas the resins were 5208, BP907, 4901/MDA, and 4091/mPDA.

The predominant macroscopic failure mode has been identified as shear crippling. When the matrix resin is stiff, shear crippling is the result of fiber kinking on a microscopic scale. Microbuckling can replace kinking if the resin is soft, e.g., in T300/BP907. Microbuckling failure is a result of high bending strains in the fiber in the post-buckled state. A partial shear crippling may lead to longitudinal splitting between fibers at the tip of the shear crippling zone because of the required kinematic compatibility. Shear crippling in composites resembles slip lines in metals.

For the materials, loading rates, and test configurations studied, failure was almost always catastropic, and detecting partial failure was successful in only a very few tests. Little variation in failure mode could be seen from material to material.

The higher tensile strain property of the T700 fiber compared to the T300 fiber did not translate into improved unidirectional laminate strength. The T700 fiber has a smaller diameter which may be a factor. While the resin modulus has a small effect on the composite modulus, it has a strong effect on the composite compressive strength. Tensile properties of the composite are not affected significantly by the resin modulus. The compressive strength can at least qualitatively be predicted by a nonlinear model incorporating initial fiber curvature.

As discussed in the Appendix, the factor v_f in Eq. (28) is the result of considering the equilibrium of the forces and moments acting on the fiber itself rather than on the representative volume element consisting of the fiber and the matrix. The resulting equation yields a better estimate even when nonlinear material properties and initial curvature of fibers are not included.

ACKNOWLEDGMENTS

The first author's (H. Thomas Hahn) work was supported by the NASA Langley Research Center under Grant NAG-1-295. The authors would like to thank Mohsen Sohi for his help in conducting experimental measurements on the graphite/epoxy composites.

APPENDIX

Calculation of Distributed Moment m Applied to a Buckled Fiber

Consider the cross section of a circular fiber in a uniform shear stress field τ_{yx}, as shown in Fig. 16(a). The resultant force d_f on an infinitesimal area $r_f d\theta$ on the fiber surface is given by

$$d_f = \tau_{yx} r_f \sin\theta \, d\theta \tag{A-1}$$

The resulting moment dm about the z axis is given by

$$dm = -r_f \sin\theta \, d_f = -\tau_{yx} r_f^2 \sin^2\theta d\theta$$

Thus the total moment m per unit length of the fiber becomes

$$m = -\int_o^{2\pi} \tau_{yx} r_f^2 \sin^2\theta d\theta = -r_f^2 \tau_{yx} \int_o^{2\pi} \sin^2\theta d\theta = -\pi r_f^2 \tau_{yx} \tag{A-2}$$

In unidirectional composites τ_{yx} is replaced by τ_{LT}, and hence

$$m = -\pi \frac{d_f^2}{4} \tau_{LT} \tag{A-3}$$

where d_f is the fiber diameter, i.e., $d_f = 2r_f$. Equation (A-3) is the same as Eq. (23).

If the representative area is taken to be a rectangle as shown in Fig. 16(b), and if the shearing stress τ_{yx} is applied on the top and bottom surfaces, the moment m is simply

$$m = -(h_f + h_m) \tau_{yx} \tag{A-4}$$

In terms of the fiber volume fraction v_f, where

$$v_f = \frac{h_f}{h_f + h_m} \tag{A-5}$$

and the composite shearing stress τ_{LT}, Eq. (A-4) can be written

as

$$m = \frac{h_f}{v_f} \tau_{LT} \tag{A-6}$$

Equation (A-6) is the same as Eq. (16) when τ_{LT} is approximated by

$$\tau_{LT} = \frac{G_m}{1 - v_f} \frac{dv}{dx} \tag{A-7}$$

Since Eqs. (1) to (3) are to be solved for the buckling of a fiber, Eq. (A-3) is preferred to Eq. (A-6).

REFERENCES

1. Williams, J. G.; and Rhodes, M. D.: The Effect of Resin on the Impact Damage Tolerance of Graphite/Epoxy Laminates. NASA TM 83213, Oct. 1981.

2. Starnes, J. H., Jr.; and Williams, J. G.: Failure Characteristics of Graphite-Epoxy Structural Components Loaded in Compression. Mechanics of Composite Materials - Recent Advances. Hashin and Herakovich, Editors, Pergamon Press, 1983.

3. Hawthorne, H. M.; and Teghtsoonian, E.: Axial Compression Fracture in Carbon Fibres. J. Mat. Sci., Vol. 10, 1975, pp. 41-51.

4. Hahn, H. T.: Effects of Constituent Properties on Compression Failure Mechanisms. Presented at the Tough Composite Materials Workshop, NASA Langley Res. Center, May 1983. NASA CP-2334, 1984.

5. Chiao, C. C.; and Chiao, T. T.: Aramid Fibers and Composites. Handbook of Composites, G. Lubin, Ed., 1982, pp. 272-317.

6. Greszczuk, L. B.: On Failure Modes of Unidirectional Composites Under Compressive Loading. Proc. of 2nd USA-USSR Symp. on Fracture of Composite Materials, G. C. Sih, Ed., 1981, pp. 231-246.

7. Kulkarni, S. V.; Rice, J. R.; and Rosen, B. W.: An Investigation of the Compressive Strength of Kevlar 49/Epoxy Composites. Composites, Vol. 6, 1975, pp. 217-225.

8. Weaver, C. W.; and Williams, J. G.: Deformation of a Carbon-Epoxy Composite Under Hydrostatic Pressure. J. Mat. Sci., Vol. 10, 1975, pp. 1323-1333.

9. Chaplin, C. R.: Compressive Fracture in Unidirectional Glass-Reinforced Plastics. J. Mat. Sci., Vol. 12, 1977, pp. 347-352.

10. Evans, A. G.; and Adler, W. F.: Kinking as a Mode of Structural Degradation in Carbon Fiber Composites. Acta Met., Vol. 26, 1978, pp. 725-738.

11. Hancox, N.: The Compression Strength of Unidirectional Carbon Fibre Reinforced Plastic. J. Mat. Sci., Vol. 10, 1975, pp. 234-242

12. Sadowsky, M. A.; Pu, S. L.; and Hussain, M. A.: Buckling of Microfibers. J. Appl. Mech., Vol. 34, 1967, pp. 1011-1016.

13. Herrman, L. R.; Mason, W. E.; and Chan, T. K.: Response of Reinforcing Wires to Compressive States of Stress. J. Comp. Mat., Vol 1., 1967, pp. 212-226.

14. Lanir, Y.; and Fung, Y. C. B.: Fiber Composite Columns Under Compression. J. Comp. Mat., Vol. 6, 1972, pp. 387-401.

15. Greszczuk, L. B.: Microbuckling of Unidirectional Composites. AFML-TR-71-231, Jan. 1972.

16. Rosen, V. W.: Mechanics of Composite Strengthening in Fiber Composite Materials, ASM, 1965, pp. 37-75.

17. Schuerch, H.: Prediction of Compressive Strength in Uniaxial Boron Fibre-Metal Matrix Composite Materials. AIAA J., Vol. 4, 1966, pp. 102-105.

18. Greszczuk, L. B.: Microbuckling Failure of Circular Fiber Reinforced Composites. AIAA J., Vol 13, 1975, pp. 1311-1318.

19. Davis, J. G., Jr.: Compressive Strength of Fiber REinforced Composite Materials. Composite Reliability, ASTM STP 580, 1975, pp. 364-377.

20. Wang, A. S. D.: Non-Linear Microbuckling Model Predicting the Compressive Strength of Unidirectional Composites. ASME Paper 78-WA/Aero-1, 1978.

21. Budiansky, B.: Micromechanics. Computers & Structures, Vol. 16, 1983, pp. 1-4.

22. Argon, A. S.: Fracture of Composites. In Treatise of Materials Science and Technology, Vol. 1, Academic Press, 1972.

23. Hanasaki, S.; and Hasegawa, Y.: Compressive Strength of Unidirectional Fibrous Composites. J. Comp. Mat., Vol. 8, 1974, pp. 306-309.

24. Sinclair, J. H.; and Chamis, C. C.: Compressive Behavior of Unidirectional Fibrous Composites. Compression Testing of Homogeneous Materials and Composites, ASTM STP 808, R. Chait and R. Papirno, Eds., ASTM, 1983, pp. 155-174.

25. Adsit, N. R.: Compression Testing of Graphite/Epoxy. Compression Testing of Homogeneous Materials and Composites, ASTM STP 808, R. Chait and R. Papirno, Eds., ASTM, 1983, pp. 175-186.

26. Palmer, R. J.: Investigation of the Effect of Resin Material on Impact Damage to Graphite/Epoxy Composites. NASA CR 165677, March 1981.

27. Tsai, S. W.; and Hahn, H. T.: Introduction to Composite Materials, Technomic Pub. Co., Lancaster, PA, 1980.

28. Popov, E. P.: Mechanics of Materials. 2nd ed., Prentice-Hall, 1976.

Table 1. Geometric Parameters for Kink Band

Material	β	δ/d_f	Reference
Gr/Ep	22 - 26°	~3	[7]
	45°		[10]
Carbon/Carbon	24 - 28°	~7	[9]
Gl/Ep	20 - 30°		[8]
Kv 49/Ep	55 - 60°		[6]
	$\alpha \approx 2\beta$		[8]

Table 2. Constituent Materials

Fiber	Matrix	Fiber Weight Content, %	Laminate Nominal Thickness, mm
T300	Narmco 5208	59	3.6
	American Cyanamid BP 907	60	3.9
	Union Carbide 4901/MDA	68	3.0
	Union Carbide 4901/mPDA	71	3.0
T700	BP 907	60	3.6
	4901/MDA	66	3.6
	4901/mPDA	65	3.6

Identification of commercial products and companies in the report is used to describe adequately the test materials. The identification of these commercial products does not constitute endorsement, expressed or implied, of such products by the National Aeronautics and Space Administration.

Table 3. Nominal Properties of Constituent Materials

Material	Diameter, μm	Modulus[1], GPa	Failure[1] Stress, MPa	Failure[1] Strain, %
T300	7.0	230	3310	1.4
T700	5.1	238	4550	1.9
5208	-	4.00	57.2	1.8
BP907	-	3.10	89.5	4.8
4901/MDA	-	4.62	103.4	4.0
4901/mPDA	-	5.46	115.1	2.4

[1] In tension

Table 4. Linear Regression Analysis[a] for the Data of Reference [25]

y	a	b	Correlation Coefficient
Compressive modulus	7.091	101.0	0.4674
Tensile modulus	4.392	123.4	0.2898
Compressive strength	0.433	-0.1685	0.9021
Tensile strength	0.068	1.586	0.2592
Flexural strength	0.423	0.600	0.7764

[a] $y = ax + b$; x = resin tensile modulus

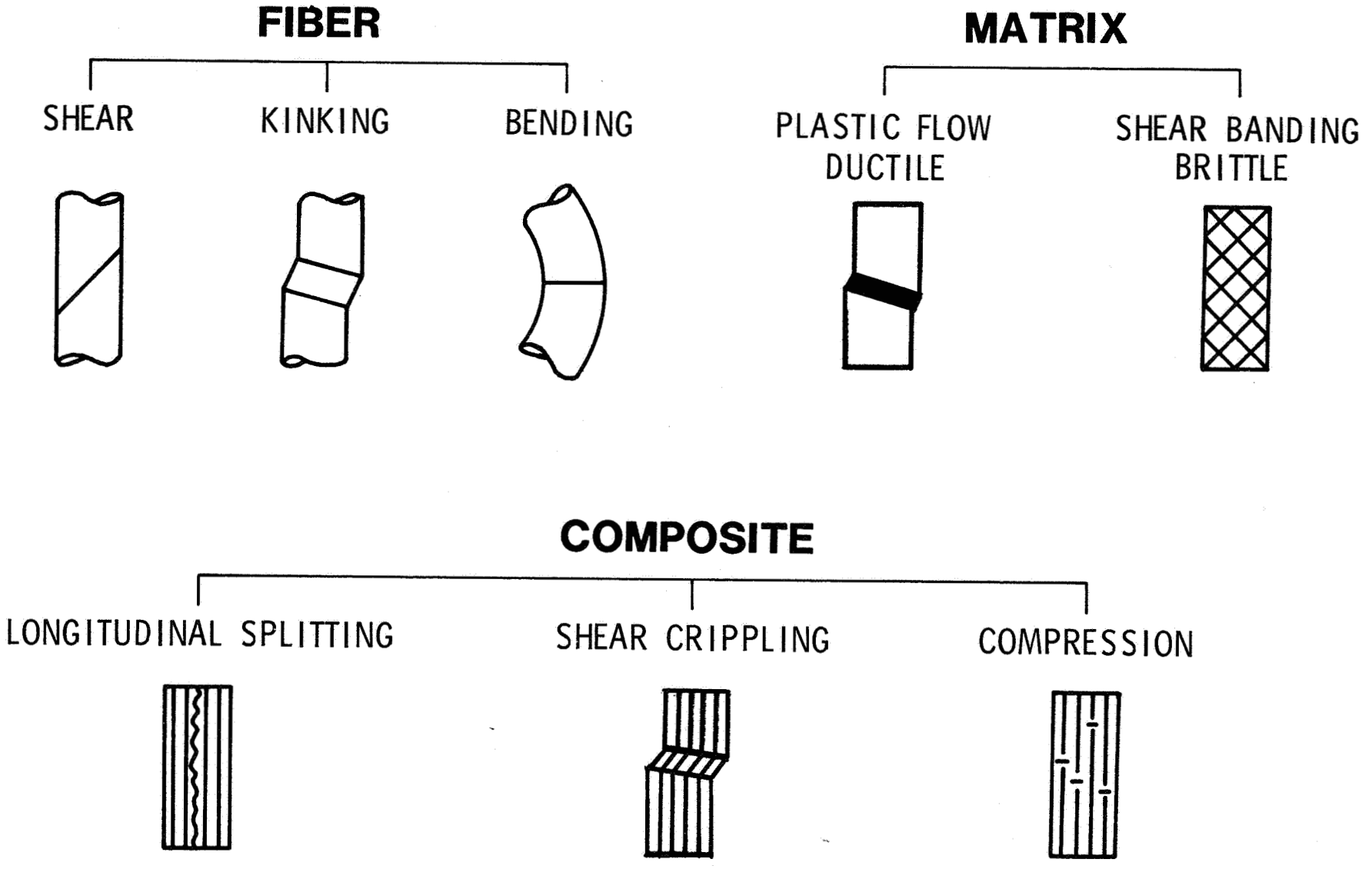

Figure 1. Composite compression failure modes.

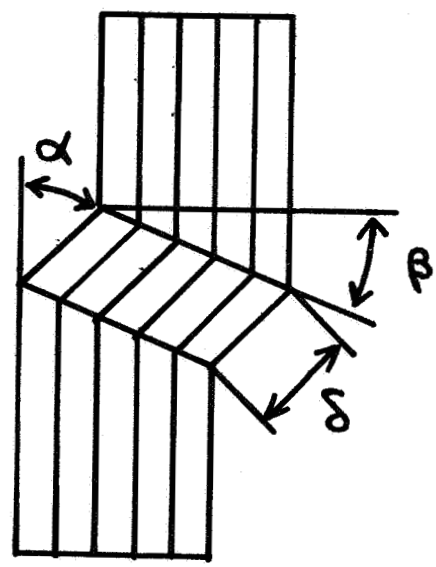

Figure 2. Kink band geometry.

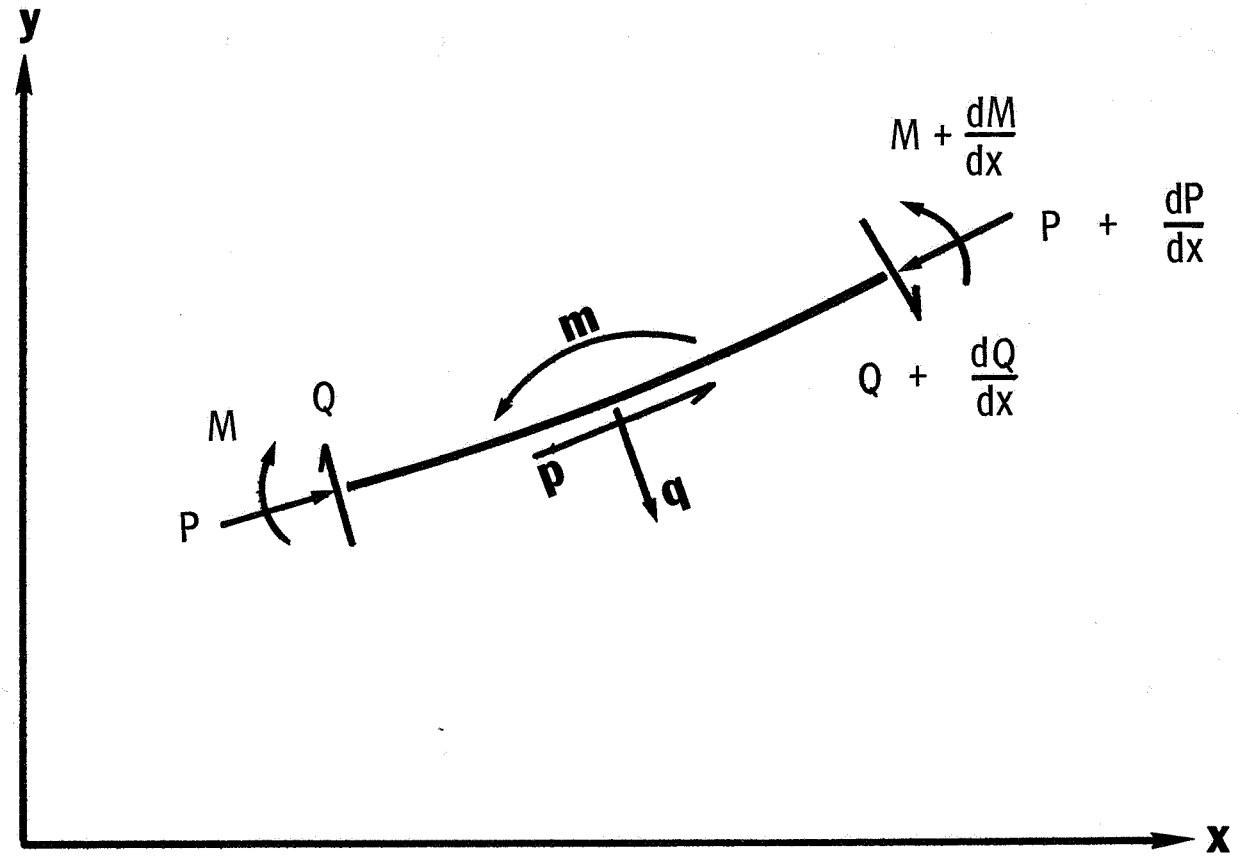

Figure 3. Free body diagram for a fiber segment.

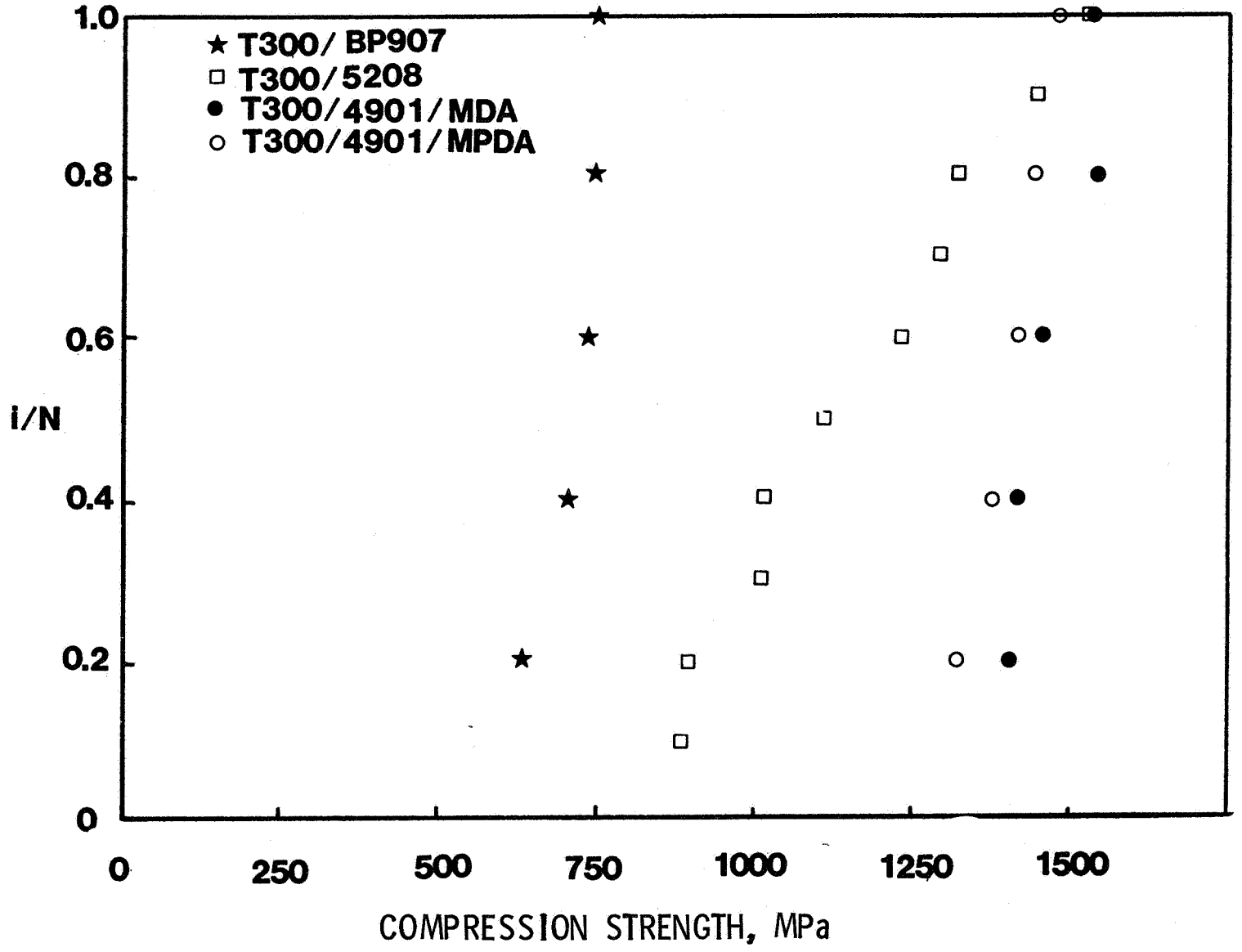

Figure 4. Strength distributions for T300 composites.

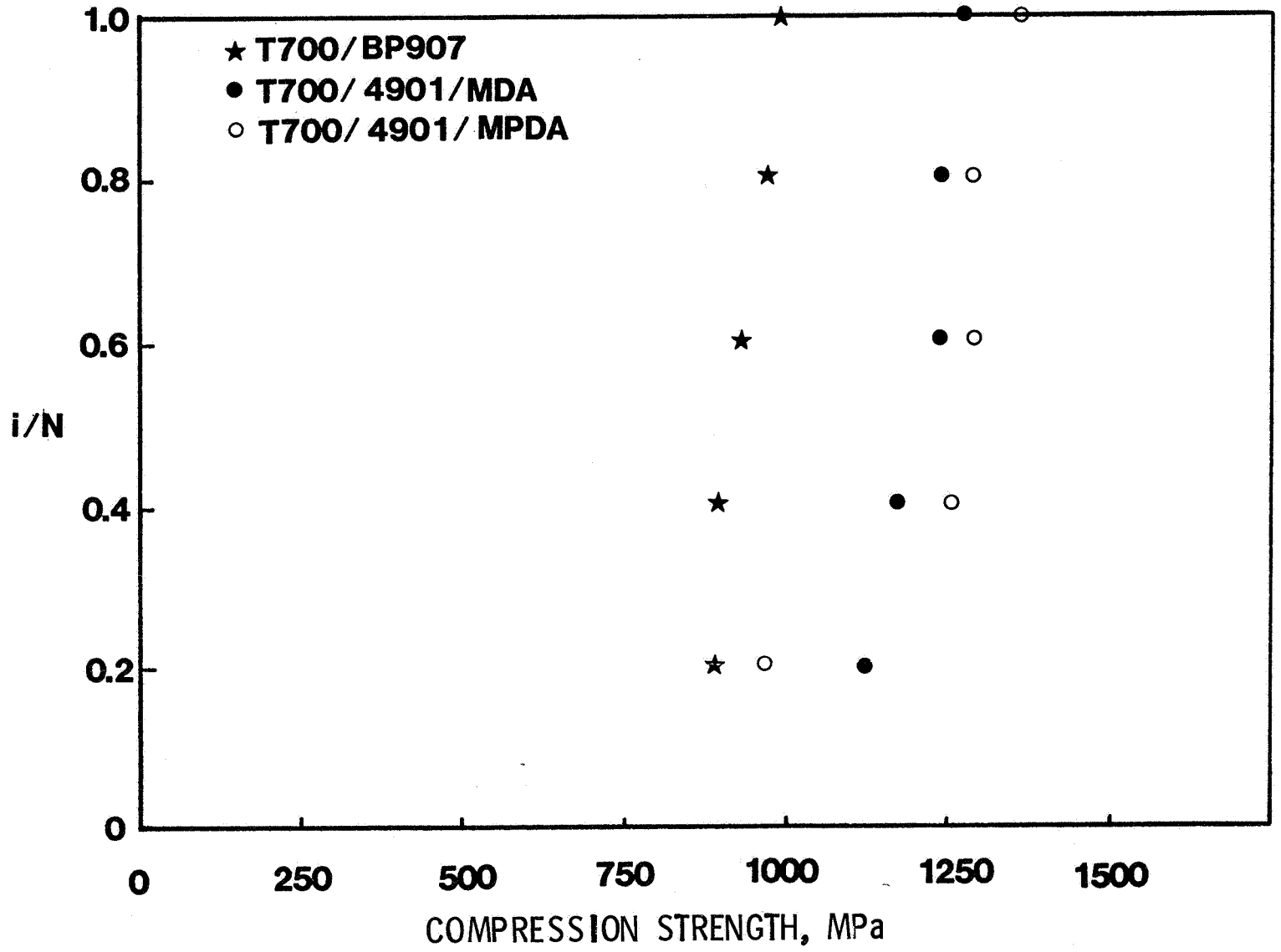

Figure 5. Strength distributions for T700 composites.

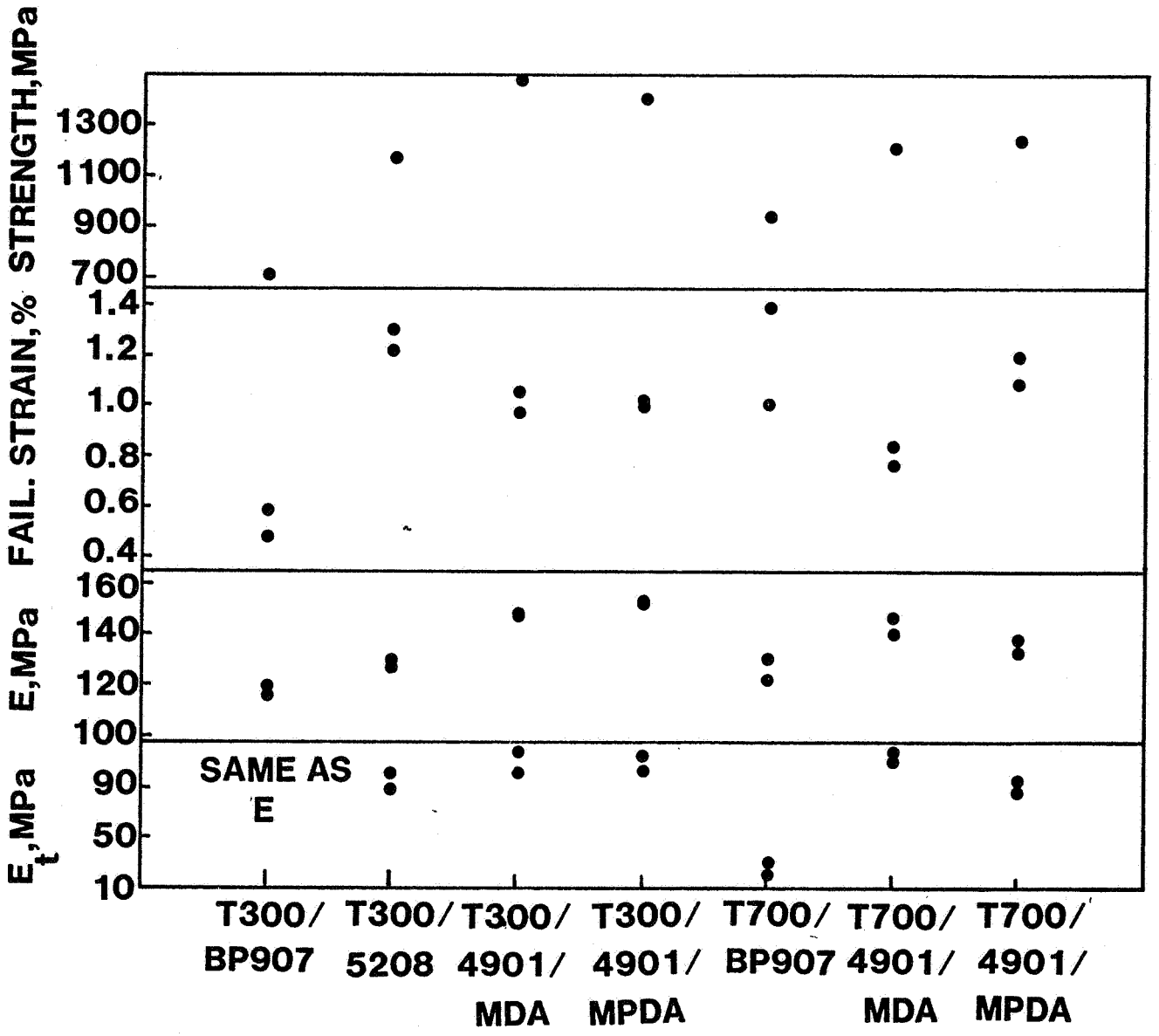

Figure 6. Comparison of unidirectional laminate properties.

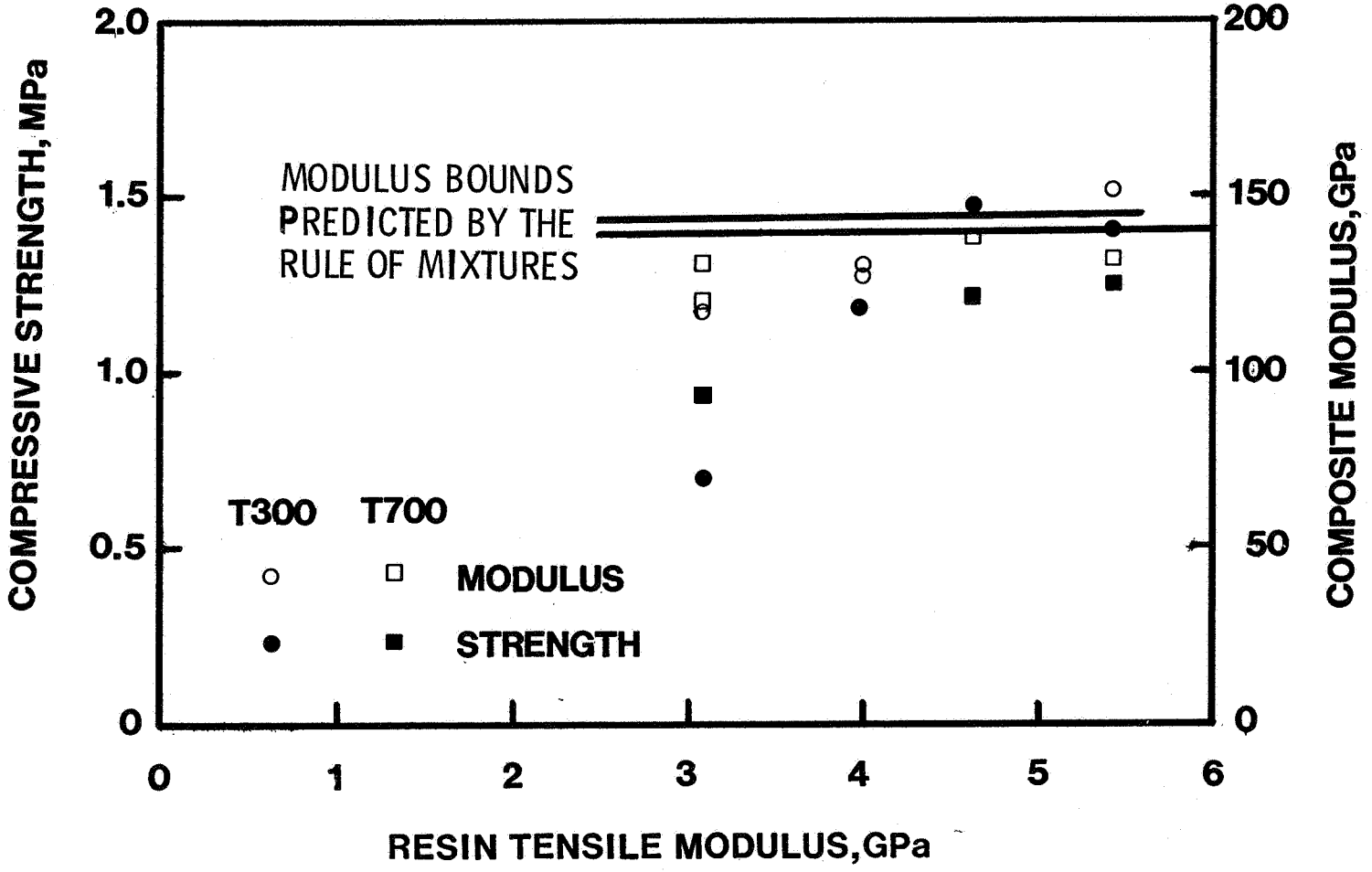

Figure 7. Effect of resin tensile modulus on modulus and strength of T300 and T700 composites under compression.

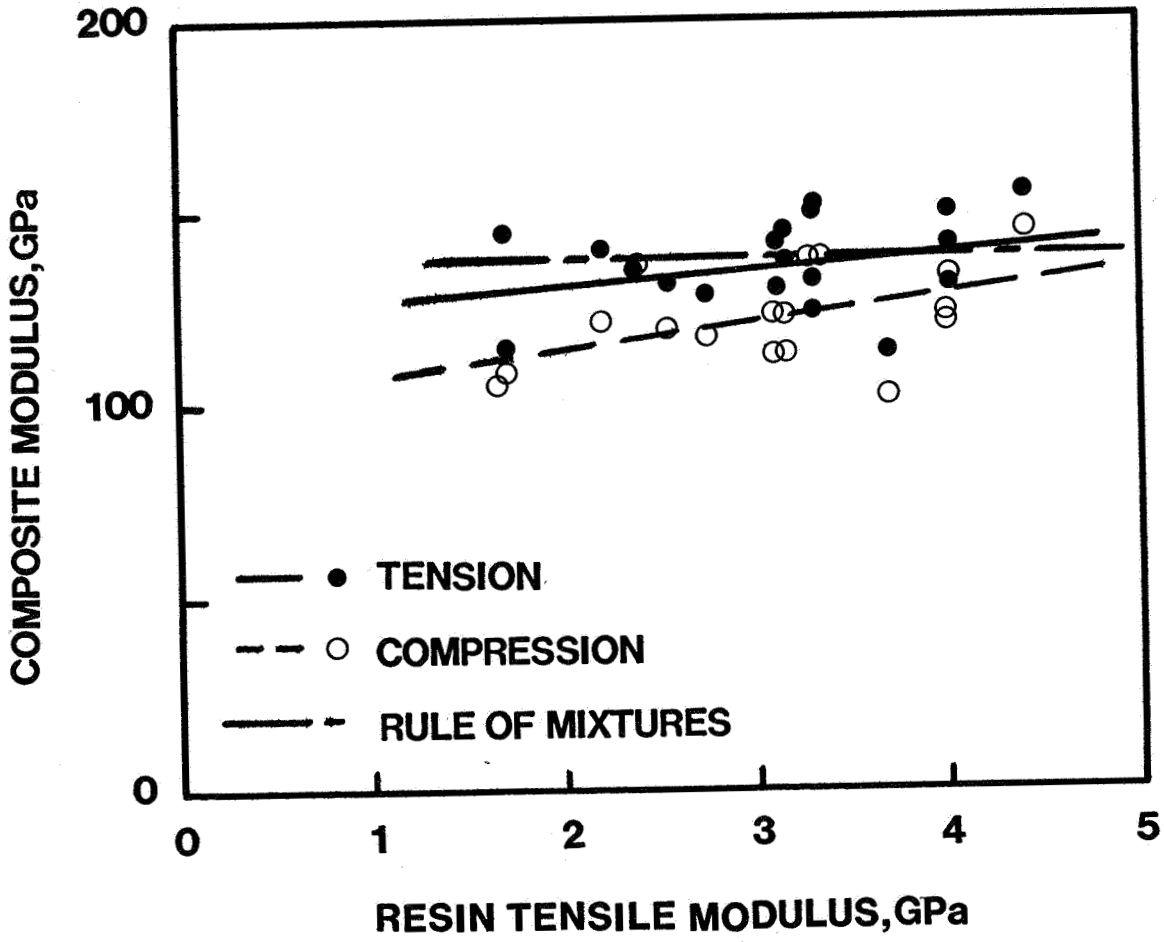

Figure 8. Effect of resin tensile modulus on composite moduli (data from [25]).

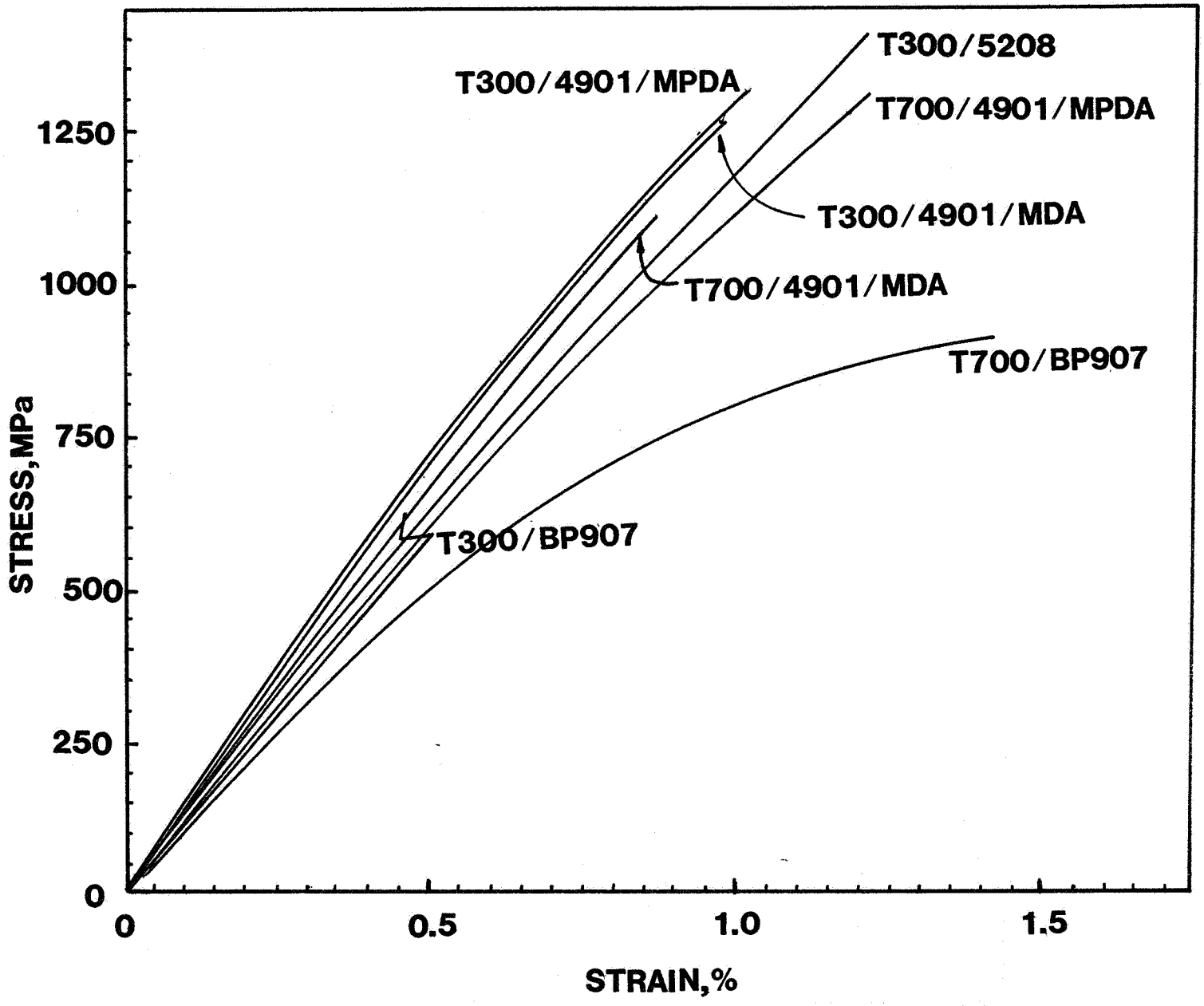

Figure 9. Compressive stress-strain curves for T300 and T700 composites.

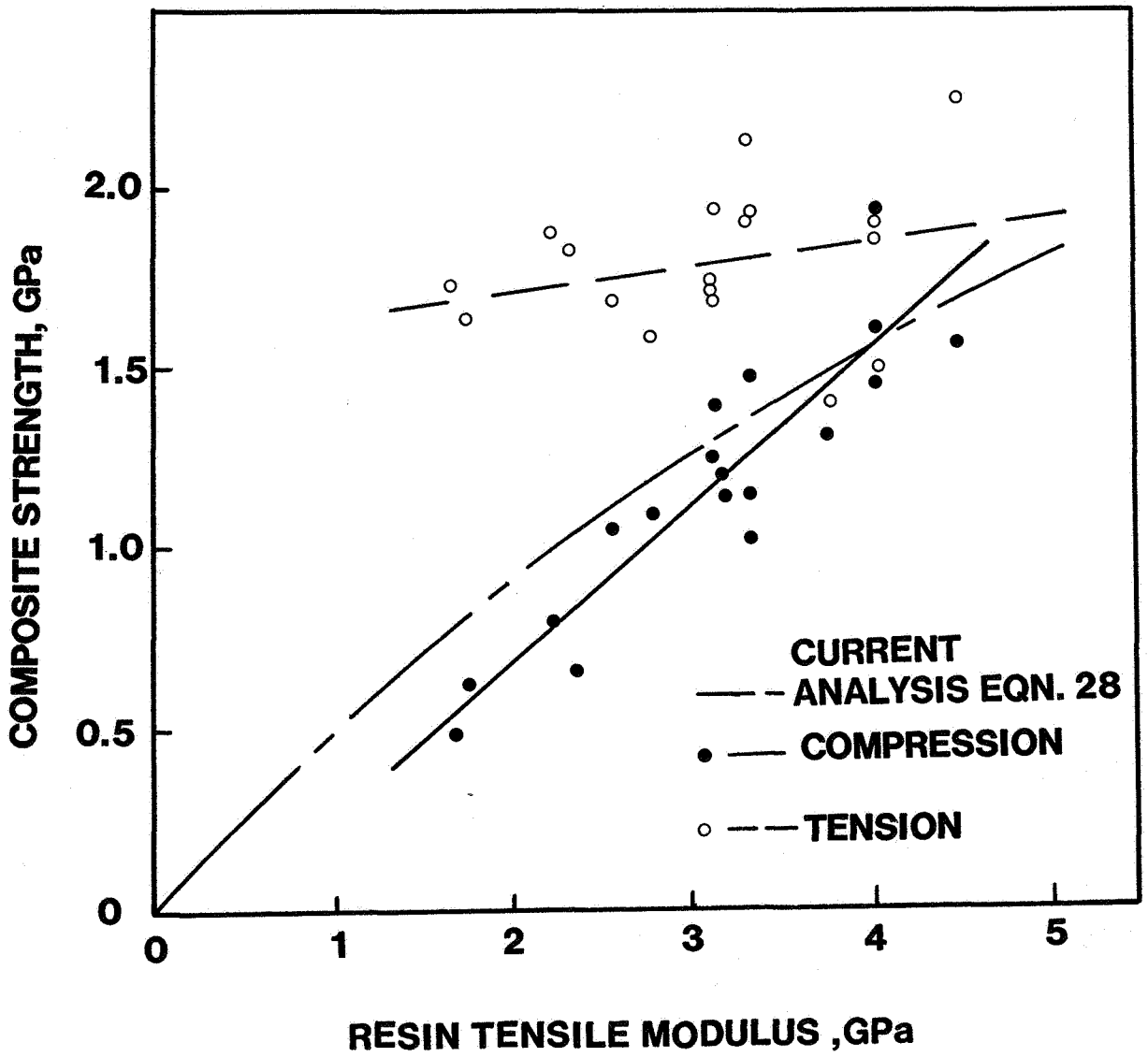

Figure 10. Effect of resin tensile modulus on composite strengths (data from [25]).

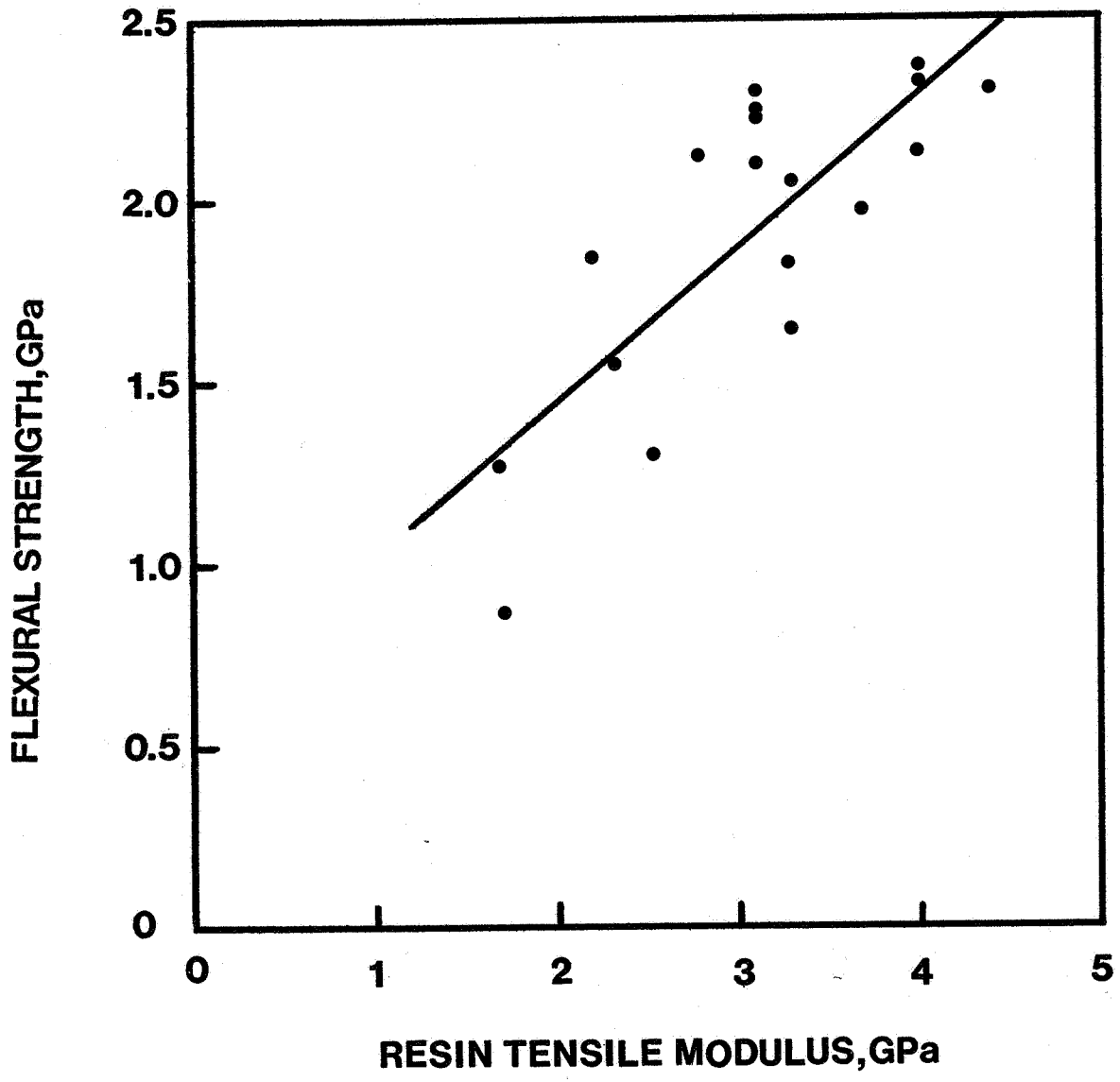

Figure 11. Effect of resin tensile modulus on flexural strength (data from [25].

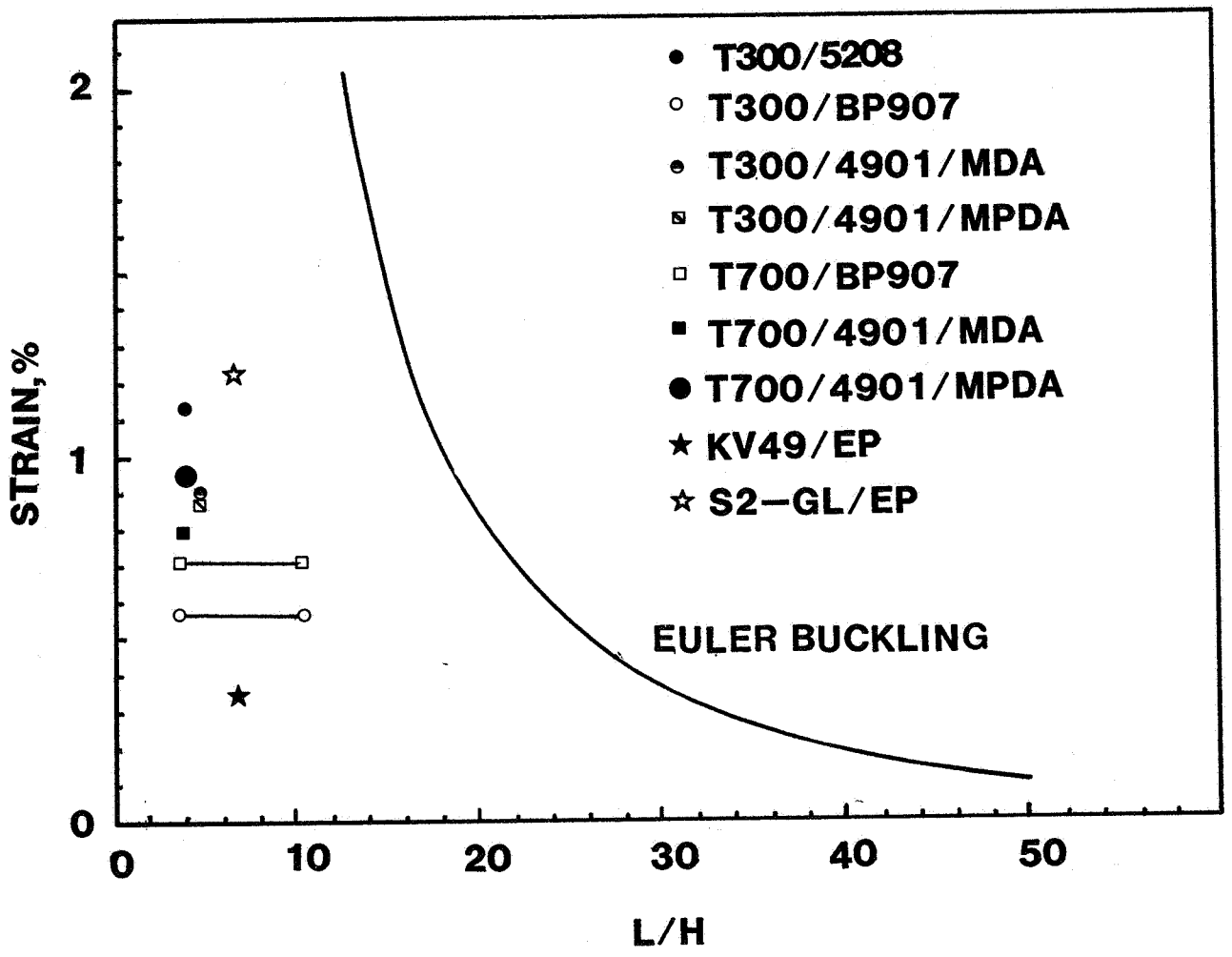

Figure 12. Effect of span-to-thickness ratio on compression failure strain.

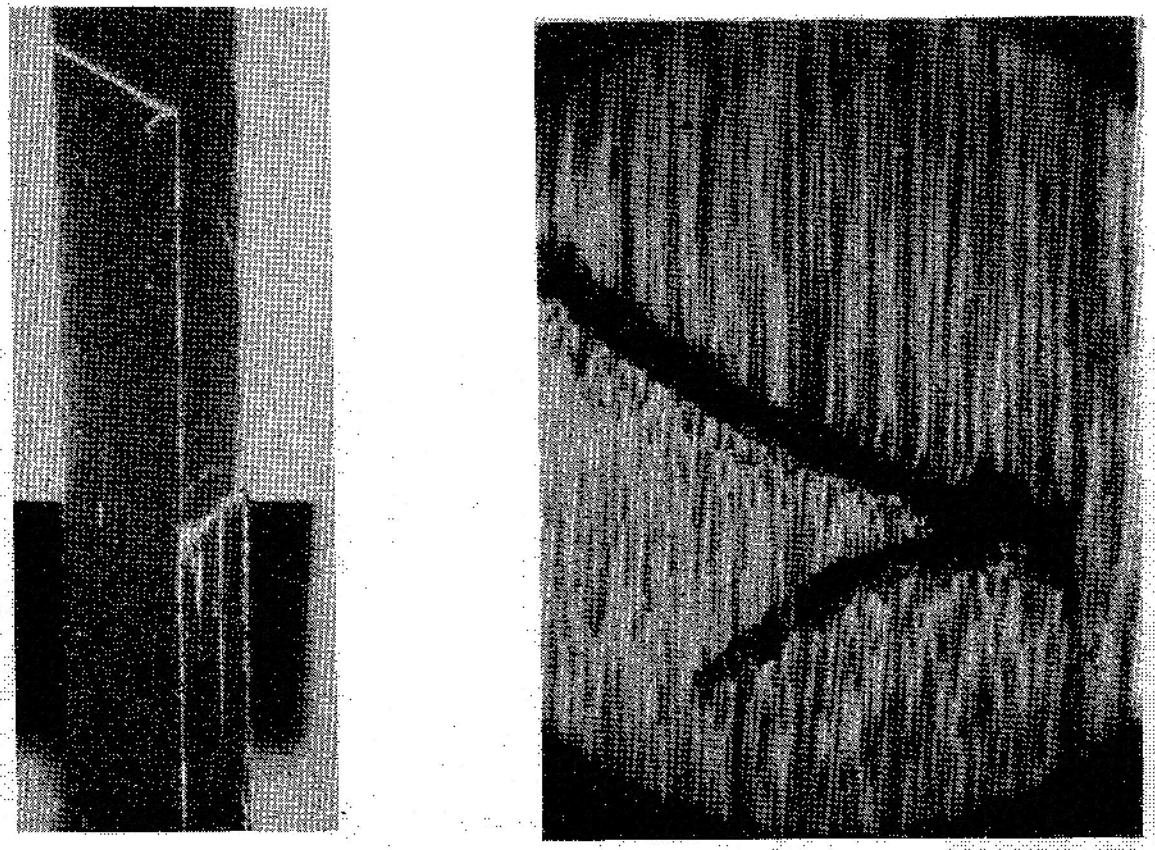

(a) Overall edge view.

(b) Tip of kink bands.

Figure 13. Partial failure in a T300/5208 specimen loaded to 1028 MPa.

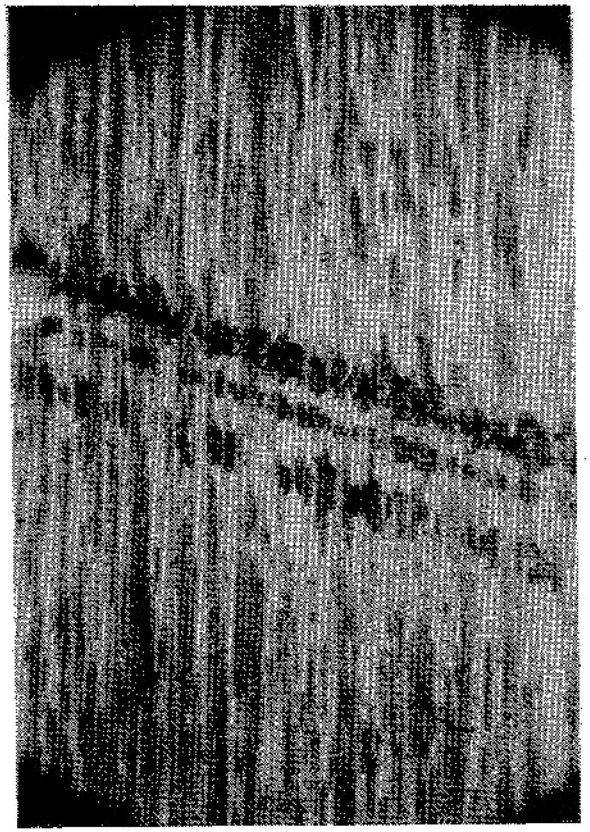

(a) Overall edge view.

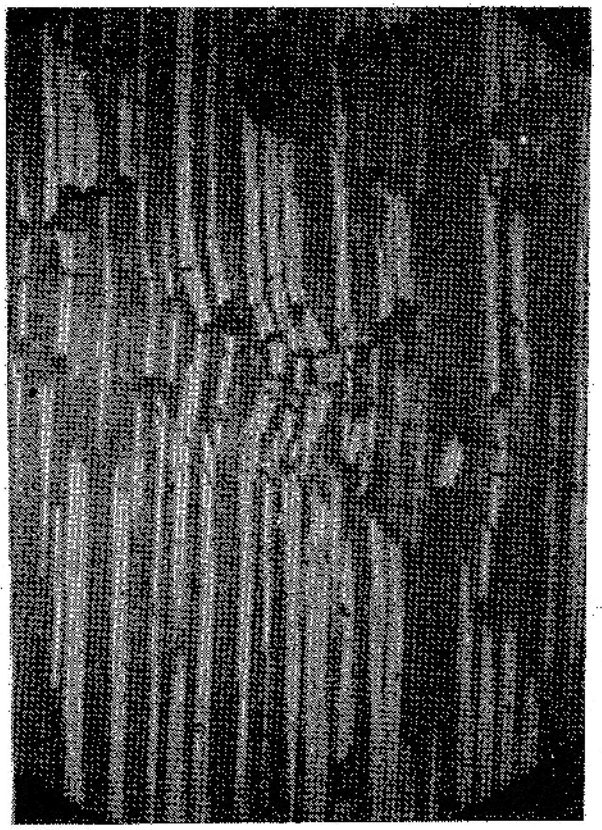

(b) Microbuckling of fibers in a shear crippling zone.

(c) Tip of microbuckling band.

Figure 14. Partial failure in a T300/BP907 specimen.

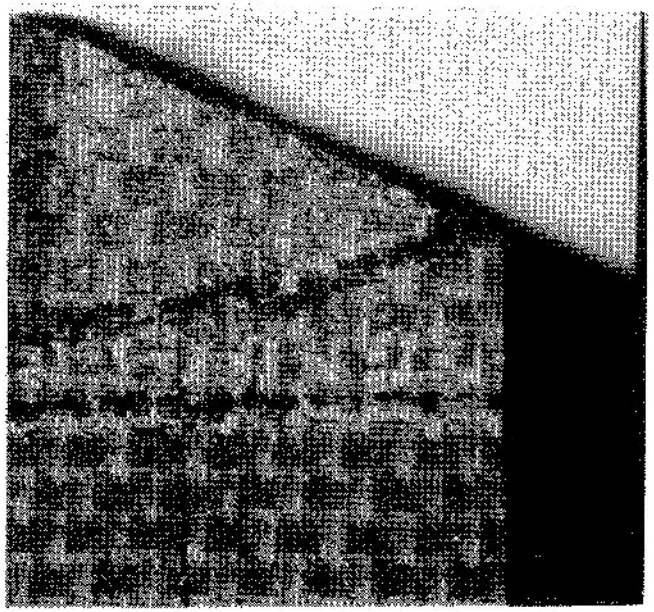

(a) Across-the-width.

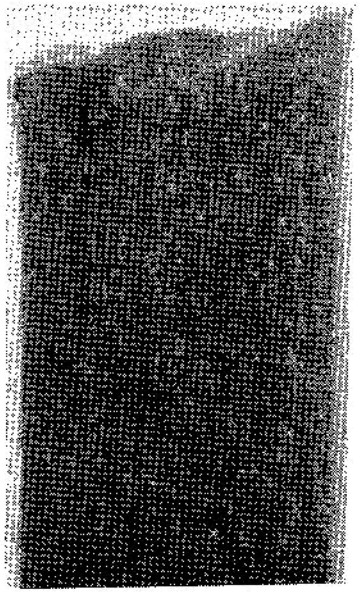

(b) Through-the-thickness.

Figure 15. Modes of shear crippling.

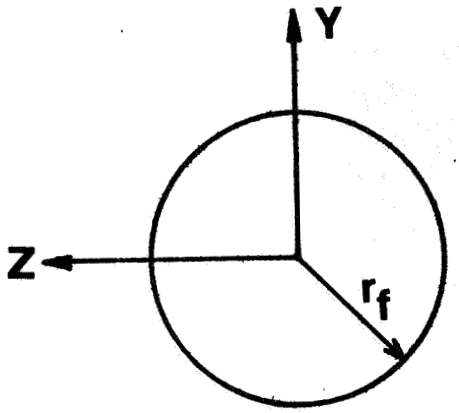

(a) A circular fiber.

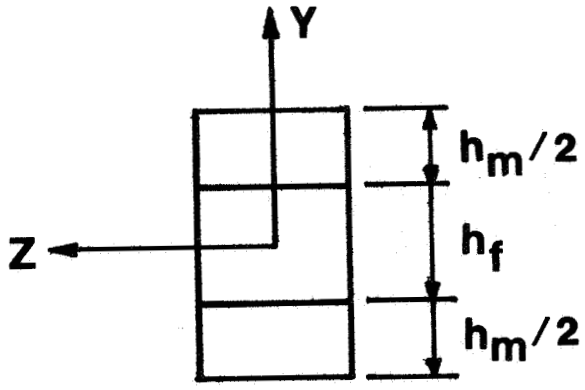

(b) A rectangular fiber.

Figure 16. Representative cross-sectional area.

1. Report No.	2. Government Accession No.	3. Recipient's Catalog No.
NASA TM-85834		

4. Title and Subtitle	5. Report Date
Compression Failure Mechanisms in Unidirectional Composites	August 1984
	6. Performing Organization Code 505-33-33-06

7. Author(s)	8. Performing Organization Report No.
H. Thomas Hahn[1] and Jerry G. Williams[2]	
	10. Work Unit No.
9. Performing Organization Name and Address	
NASA Langley Research Center Hampton, VA 23665	11. Contract or Grant No.
	13. Type of Report and Period Covered
12. Sponsoring Agency Name and Address	Technical Memorandum
National Aeronautics and Space Administration Washington, DC 20546	14. Sponsoring Agency Code

15. Supplementary Notes

Paper presented at ASTM 7th Symposium on Composite Materials, Philadelphia, PA, April 2-4, 1984.

1. Washington, University - St. Louis, MO 2. NASA Langley Research Center - Hampton,VA

16. Abstract

The paper examines compression failure mechanisms in unidirectional composites. Possible failure modes of constituent materials are summarized and analytical models for fiber microbuckling are reviewed from a unified viewpoint. Due to deficiencies in available models, a failure model based on nonlinear material properties and initial fiber curvature is proposed.

The effect of constituent properties on composite compression behavior was experimentally investigated using two different graphite fibers and four different epoxy resins. The predominant macroscopic-scale failure mode was found to be shear crippling. In a soft resin, shear crippling was in the form of buckling of fibers on a microscopic scale. However, for stiff resins failure was characterized by the formation of a kink band. For unidirectional laminates, compressive strength, and compressive modulus to a lesser extent, were found to increase with increasing magnitude of resin modulus. The change in compressive strength with resin modulus was predicted using the proposed nonlinear model.

17. Key Words (Suggested by Author(s))	18. Distribution Statement
Composite Materials Composite Structures Composite Failure Graphite-Epoxy	Unclassified - Unlimited Subject Category 24

19. Security Classif. (of this report)	20. Security Classif. (of this page)	21. No. of Pages	22. Price
Unclassified	Unclassified	43	A03

For sale by the National Technical Information Service Springfield, Virginia 22161 NASA-Langley, 1984